

# Theory of Electronic Raman Scattering in Nearly Antiferromagnetic Fermi Liquids

T.P. Devereaux<sup>1</sup> and A.P. Kampf<sup>2</sup>

<sup>1</sup> *Department of Physics, George Washington University, Washington, DC 20052*

<sup>2</sup> *Theoretische Physik III, Elektronische Korrelationen und Magnetismus,  
Institut für Physik, Universität Augsburg, 86135 Augsburg, Germany*

A theory of electronic Raman scattering in nearly antiferromagnetic Fermi liquids is constructed using the phenomenological electron-electron interaction introduced by Millis, Monien, and Pines. The role of "hot spots" and their resulting signatures in the channel dependent Raman spectra is highlighted, and different scaling regimes are addressed. The effects of self consistency and vertex corrections are compared to a perturbative treatment of the interaction. The theory is then compared to Raman spectra taken in the normal state of cuprate superconductors, and it is shown that many features of the symmetry dependent spectra can be explained by the theory. Remaining questions are addressed.

PACS numbers: 74.25.Jb, 71.27.+a, 78.30-j

## I. INTRODUCTION.

Recent results from angle resolved photo-emission (ARPES) studies have shown that the planar quasiparticle (qp) dynamics in the normal state of high temperature superconductors are extremely anisotropic [1]. For optimally doped samples with the highest  $T_c$ 's, the quasiparticle spectrum observed for Fermi surface crossings along the  $(\pi, 0) - (\pi, \pi)$  direction in the Brillouin zone (BZ) is quite smeared by strong scattering compared to the observed spectrum along the  $(0, 0) - (\pi, \pi)$  direction. This anisotropy becomes more pronounced as the materials are made to be further underdoped with concomitantly lower transition temperatures into the superconducting state [2]. Understanding the nature and origin of this anisotropy could lead to a better understanding of the complex dynamics which cause the normal state of the cuprates to be very far away from being "normal".

Many theoretical efforts have been conducted to understand this planar anisotropy. These efforts usually have focused on understanding the results from photo-emission. However, as demonstrated in the superconducting state [3], electronic Raman scattering has proven to be a useful tool to understand qp dynamics on selected regions of the Fermi surface. While an average is made around the Fermi surface for most calculations of response functions (e.g. as for the penetration depth), the matrix elements for Raman scattering can be tuned by orienting incoming and outgoing photon polarizations, thereby projecting out different regions of the Fermi surface. In Ref. [3] it was shown how this tuning could be used to provide a detailed probe of the momentum dependence of the superconducting energy gap throughout the BZ.

In this regard, Raman scattering can be considered a complementary probe to ARPES. Raman measurements on several systems have shown a remarkable *channel* dependence in the normal state for the optimally- and under-doped cuprates in a variety of systems [4–6]. For scattering geometries of  $B_{1g}$  symmetry, an almost

temperature independent Raman spectrum has been observed at low frequencies, while for  $B_{2g}$  orientations the spectra show a temperature dependence that tracks that of the DC resistivity [5]. Moreover, the overall magnitude of the electronic continuum is observed to be relatively independent of doping for the  $B_{2g}$  channel, but decreases dramatically with underdoping for the  $B_{1g}$  channel. One is tempted to conclude that the qps near  $(\pi, 0)$  which are probed by the  $B_{1g}$  channel are particularly incoherent. Coupled to the flatness of the bands there, these qps are likely not to participate in transport [7]. Currently there is no theoretical understanding of Raman scattering in the normal state of the cuprates, as all previous theories failed to predict large differences between these two channels at low frequencies. It is the purpose of this paper to address these issues.

It is widely believed that strong antiferromagnetic (AF) correlations are an important ingredient needed to describe the unusual properties found in the normal state of the cuprate superconductors and perhaps therein lies the origin of the strongly anisotropic dynamics in the cuprates. Large qp scattering for momentum transfers near the AF wave-vector have been invoked to explain the photo-emission results [8]. Therefore we have studied the phenomenological Nearly Antiferromagnetic Fermi Liquid (NAFL) model [9] as an example of highly anisotropic scattering to investigate the two-particle Raman response. Our results show that the Raman response is an ideal probe to clarify the nature of qp dynamics on regions of the Fermi surface.

The outline of the paper is as follows: Section II reviews and outlines a generalized approach to calculate non-resonant Raman scattering in correlated electron systems and introduces the model interaction. Section III investigates the NAFL model using simple perturbation theory. The scattering rate for quasiparticles on different regions of the Fermi surface is calculated and the subsequent Raman response is obtained. Section IV compares the results of the calculations in Section III to data on overdoped  $\text{Bi}_2\text{Sr}_2\text{CaCu}_2\text{O}_{8+\delta}$  (BSCCO). Section

V investigates the role of a self consistent treatment of the interaction and the role of vertex corrections. Finally Section VI summarizes our results and states our conclusions.

## II. FORMALISM.

The intensity of inelastically scattered light can be written in terms of a differential photon scattering cross section as

$$\frac{\partial^2 \sigma}{\partial \omega \partial \Omega} = \frac{\omega_S}{\omega_I} r_0^2 S_{\gamma\gamma}(\mathbf{q}, \omega),$$

$$S_{\gamma\gamma}(\mathbf{q}, \omega) = -\frac{1}{\pi} [1 + n(\omega)] \text{Im} \chi_{\gamma\gamma}(\mathbf{q}, \omega). \quad (1)$$

Here  $r_0 = e^2/mc^2$  is the Thompson radius,  $\omega_I, \omega_S$  are the frequency of the incoming and scattered photon, respectively, and we have set  $\hbar = k_B = 1$ .  $S_{\gamma\gamma}$  is the generalized structure function, which is related to the imaginary part to the Raman response function  $\chi_{\gamma\gamma}$  through the fluctuation-dissipation theorem, the second part of Eq. (1).  $n(\omega)$  is the Bose-Einstein distribution function. The Raman response measures “effective density” fluctuations,

$$\chi(i\omega) = \int_0^{1/T} d\tau e^{-i\omega\tau} \langle T_\tau [\tilde{\rho}(\tau) \tilde{\rho}(0)] \rangle, \quad (2)$$

with  $T_\tau$  the time-ordering operator and the imaginary part is obtained by analytic continuation,  $i\omega \rightarrow \omega + i0^+$ .

The Raman intensity can be represented as a scattering off an effective charge density [10]

$$\tilde{\rho} = \sum_{\mathbf{k}, \sigma} \gamma(\mathbf{k}) c_\sigma^\dagger(\omega_I, \omega_S; \mathbf{k}) c_\sigma(\mathbf{k}), \quad (3)$$

where  $\sigma$  is the spin index,  $\gamma(\mathbf{k})$  is the Raman scattering amplitude, and  $\omega_{I,S}$  is the frequency of the incident, scattered photon, respectively. The effective charge density is a nonconserving quantity in contrast to the real charge [11]. Here the Raman vertices  $\gamma$  are related to the incident and scattering photon polarization vectors  $\mathbf{e}^{I,S}$ , resulting from a coupling of both the charge current and the charge density to the vector potential. In general the Raman vertex depends non-trivially on both the incident and scattered photon frequencies. According to Abrikosov and Genkin [12], if the energy of the incident and scattered frequencies  $\omega_I, \omega_S$  are negligible compared to the energy band gap,  $\gamma$  can be expressed in terms of the curvature of the bands and the incident and scattered photon polarization vectors  $\mathbf{e}^{I,S}$  as

$$\lim_{\omega_I, \omega_S \rightarrow 0} \gamma(\mathbf{k}) = \sum_{\mu, \nu} e_\mu^I \frac{\partial^2 \epsilon(\mathbf{k})}{\partial k_\mu \partial k_\nu} e_\nu^S, \quad (4)$$

where terms of the order of  $1 - \omega_S/\omega_I$  are dropped. This expression is valid given that the incoming laser light

cannot excite direct band-band transitions. However one might question the appropriateness of this approximation for the cuprates given that typical incoming laser frequencies are on the order of 2 eV - certainly on the order of the relevant electronic energy scale for a single band.

An alternative approach is based on the experimental observation that the spectra in the normal state near optimal doping for a wide range of cuprate materials depend only mildly on the incoming laser frequency [13]. Since the polarization orientations transform as various elements of the point group of the crystal, one can use symmetry to classify the scattering amplitude, viz.

$$\gamma(\mathbf{k}; \omega_I, \omega_S) = \sum_L \gamma_L(\omega_I, \omega_S) \Phi_L(\mathbf{k}), \quad (5)$$

where  $\Phi_L(\mathbf{k})$  are either Brillouin zone (B.Z.H., orthogonal over the entire Brillouin zone) or Fermi surface (F.S.H., orthogonal on the Fermi surface only) harmonics which transform according to point group transformations of the crystal [14]. Representing the magnitude but not the  $\mathbf{k}$ -dependence of scattering, the prefactors can be approximated to be frequency independent and taken as model constants to fit absolute intensities.

Thus we have simplified the many-band problem in terms of symmetry components which can be related to charge degrees of freedom on portions of the Fermi surface. While sacrificing information pertaining to overall intensities, we have gained the ability to probe and compare excitations on different regions of the Fermi surface based solely on symmetry classifications. This can be illustrated by considering the various experimentally accessible polarization orientations.

Using an  $x, y$  coordinate system locked to the  $\text{CuO}_2$  planes, incident and scattered light polarizations aligned along  $\hat{x} + \hat{y}, \hat{x} - \hat{y}$  for example transform according to  $B_{1g}$  symmetry, and thus

$$\Phi_{B_{1g}}(\mathbf{k}) = \cos(k_x a) - \cos(k_y a) + \dots, \quad (6)$$

where  $\dots$  are higher order B.Z.H. Likewise,  $\mathbf{e}^{I,S}$  aligned along  $\hat{x}, \hat{y}$  transforms as  $B_{2g}$ :

$$\Phi_{B_{2g}}(\mathbf{k}) = \sin(k_x a) \sin(k_y a) + \dots \quad (7)$$

The  $A_{1g}$  basis function is

$$\Phi_{A_{1g}}(\mathbf{k}) = a_0 + a_2 [\cos(k_x a) + \cos(k_y a)] + a_4 \cos(k_x a) \cos(k_y a) + a_6 [\cos(2k_x a) + \cos(2k_y a)] + \dots, \quad (8)$$

with the expansion parameters  $a_i$  determined via a fitting procedure with experiment [15]. The  $A_{1g}$  response is not directly accessible from experiments and must be obtained by subtracting several combinations of the response for various polarization orientations.

By considering the  $\mathbf{k}$ -dependence of the basis functions, it is clear that the  $B_{1g}$  part of the spectra essentially probes light scattering events along the  $k_x$  or  $k_y$

axes,  $B_{2g}$  probes the diagonals, and  $A_{1g}$  is more of an average over the entire Brillouin zone. It is in this manner that information about the momentum dependence of the quasiparticle scattering rate can be obtained.

Since the momentum transfer by the photon is negligible compared to the momentum of the electrons in metals, we are interested in the  $\mathbf{q} = 0$  Raman response. With the approximations above, the gauge invariant Raman response is of the form

$$\chi_{\gamma,\gamma}(\mathbf{q} = \mathbf{0}, i\Omega) = -\frac{T}{N} \sum_{i\omega} \sum_{\mathbf{k}} \gamma(\mathbf{k}) G(\mathbf{k}, i\omega) G(\mathbf{k}, i\omega + i\Omega) \tilde{\gamma}(\mathbf{k}, i\omega, i\omega + i\Omega), \quad (9)$$

with the renormalized vertex obeying a Bethe-Salpeter equation  $\tilde{\gamma}$

$$\tilde{\gamma}(\mathbf{k}, i\omega, i\omega + i\Omega) = \gamma(\mathbf{k}) + \frac{T}{N} \sum_{i\omega'} \sum_{\mathbf{k}'} V(\mathbf{k} - \mathbf{k}', i\omega - i\omega') \times G(\mathbf{k}', i\omega') G(\mathbf{k}', i\omega' + i\Omega) \tilde{\gamma}(\mathbf{k}', i\omega', i\omega' + i\Omega). \quad (10)$$

In the absence of vertex corrections to the Raman vertex  $\gamma(\mathbf{k})$ , the Raman response is given by

$$\chi''_{\gamma,\gamma}(\mathbf{q} = \mathbf{0}, \Omega) = \frac{2}{N} \sum_{\mathbf{k}} \gamma^2(\mathbf{k}) \int \frac{d\omega}{\pi} [f(\omega) - f(\omega + \Omega)] \times G''(\mathbf{k}, \omega) G''(\mathbf{k}, \omega + \Omega). \quad (11)$$

Here the Green's function is given in terms of the self energy  $\Sigma$  by Dyson's equation,  $G(\mathbf{k}, \omega) = [\omega - \varepsilon(\mathbf{k}) - \Sigma(\mathbf{k}, \omega)]^{-1}$ , using a 2-D tight binding band structure  $\varepsilon(\mathbf{k}) = -2t[\cos(k_x a) + \cos(k_y a)] + 4t' \cos(k_x a) \cos(k_y a) - \mu$ . From now on we set the lattice constant  $a = 1$ . We are now in a position to evaluate  $\Sigma$  and then to construct the Raman cross section.

### III. PERTURBATION THEORY AND ROLE OF SCATTERING.

#### A. Other models.

Before we introduce the NAFL portion of the calculation, we start by considering the simple form for the Raman response given in Eq. (11). We first consider non-interacting free electrons, such that the self energy can be neglected completely. In that case, the imaginary part of the Green's functions are simply  $\delta$  functions, and thus the  $q \rightarrow 0$  Raman response is given essentially by the Lindhard function, weighted by the Raman vertex. Since for  $q = 0$  there is no phase space available to create electron-hole pairs at low energies, this limit would yield no Raman cross section. Thereby, it is crucial to have a non-zero self energy in order observe inelastic light scattering at all in this limit.

Zawadowski and Cardona considered free electrons in the presence of a potential due to impurities [16]. Using Eq. (10) and assuming mainly isotropic impurity

scattering,  $\Sigma(\mathbf{k}, \omega) = -i/\tau_{L=0}$ , as well as a separable interaction diagonal in Fermi surface harmonics  $\phi_L$ ,  $V(\mathbf{k} - \mathbf{k}') = V_{\mathbf{k},\mathbf{k}'} = \sum_L V_L \phi_L(\mathbf{k}) \phi_L^*(\mathbf{k}')$ , the resulting cross section can be written in a Lorentzian form:

$$\chi''_L(\Omega) = 2N_F \gamma_L^2 \frac{\Omega \tau_L^*}{1 + (\Omega \tau_L^*)^2}, \quad (12)$$

where a flat band with density of states per spin at the Fermi level  $N_F$  has been assumed, and  $1/\tau_L^* = 1/\tau_{L=0} - 1/\tau_L$  is the impurity scattering rate in channel  $L$  reduced by vertex corrections. Finally  $\gamma_L$  is the prefactor of the Raman vertex in channel  $L$  (see Eq. 5). While impurities do yield a channel dependent response, since the spectra have a peak at the scattering rate and then falls off at large  $\omega$ , it cannot fit the large flat continuum observed in Raman experiments extending up to the scale of a few eVs [4–6].

A form similar to Eq. (12) has been obtained for the case of quasiparticle scattering in a nested Fermi liquid [17]. The calculated spectra have the same form as (12) except that a frequency and temperature dependent scattering rate is introduced which is of the form  $1/\tau_L^* = \max\{\beta_L T, \alpha_L \omega\}$ , with channel dependent prefactors  $\beta, \alpha$ . This form for the response gives qualitatively good agreement with the observed spectra, but does not yield appreciably large differences between response functions for different channels. In principle features of the quasiparticle interaction due to nesting will be pronounced for particular momentum transfers near the nesting wavevector, and coupled with the influence of the van Hove singularity may well account for the observed scattering anisotropy. However, calculations have not been performed for model Fermi surfaces, and since the flat Raman continuum has been observed to be almost independent of band structure, one might be tempted to conclude that if nesting is present, it may not be sufficient to account for the experimentally seen behavior.

#### B. NAFL Theory.

Therefore, we now consider a form for the qp interaction due to an effective spin-fermion model interaction [9]

$$V(\mathbf{q}, \Omega) = g^2 \frac{\alpha \xi^2}{1 + (\mathbf{q} - \mathbf{Q})^2 \xi^2 - i\Omega/\omega_{sf}}. \quad (13)$$

This interaction forms the basis of the NAFL theory, and has been derived by considering the interaction of electrons to external spin degrees of freedom [18]. The self energy then is given by

$$\Sigma(\mathbf{k}, i\omega) = -\frac{T}{N} \sum_{i\omega'} \sum_{\mathbf{p}} V(\mathbf{k} - \mathbf{p}, i\omega - i\omega') G(\mathbf{p}, i\omega'), \quad (14)$$

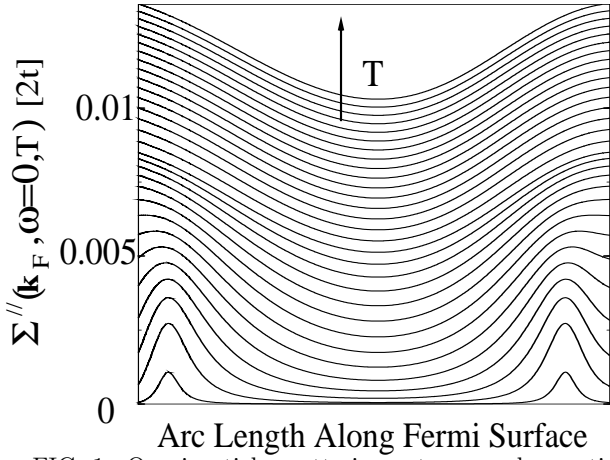


FIG. 1. Quasiparticle scattering rate around a section of the Fermi surface for different temperatures in the NAFL model. Here we have taken  $\omega_{sf}/2t = 0.00876 + 6.14T/2t$  for all  $T$  and  $\omega_{sf}\xi/2t = 0.1058$  for  $T/2t < 0.0273$  ( $z = 1$ ), and then taken  $\omega_{sf}\xi^2/2t = 0.0635$  for  $0.6 > T/2t > 0.0273$  ( $z = 2$ ).

with  $G$  the single particle Green's function. Here  $\omega_{sf}$  and  $\xi$  are the phenomenological temperature dependent spin fluctuation energy scale and the correlation length, respectively, which have been determined via fits to magnetic response data [19]. These functional parameters obey certain relations depending on different temperature and doping regimes. In the  $z = 1$  or pseudo-scaling regime, the spin correlations are strong enough to lead to changes from the classical mean field theory  $z = 2$  regime. For each scaling regime,  $\omega_{sf}\xi^z = \text{constant}$  (i.e. temperature independent).

As in Ref. [20], we use the following approximations: (i) we neglect the real part of the self energy given in (2), (ii) evaluate the Green's function at lowest order in the coupling constant  $g^2$ , (iii) neglect all vertex corrections for the Raman vertex, and (iv) momentum sums are replaced by  $\sum_{\mathbf{k}} = \int d(\Omega_{\mathbf{k}}/|\mathbf{v}_{\mathbf{k}}|) \int d\varepsilon(\mathbf{k})$ . While (iv) does not crucially affect the results, approximations (i-iii) – while simplifying the calculations – considerably miss important qp renormalizations at larger values of the coupling. Therefore we expect that these calculations would be most appropriate to describe the spectra taken on over-doped cuprate superconductors.

### 1. Quasiparticle scattering rate.

We first start by consider the effective qp scattering rate around the Fermi surface. In Fig. 1 we show the qp scattering rate, defined as the imaginary part of the self energy  $\Sigma(\mathbf{k}, \omega = 0, T)$ , around the Fermi surface as a function of temperature  $T$ . Here the calculations have been performed using the above mentioned approximations, using a value of the effective coupling constant  $\alpha g^2/2t = 6.25$ . As a result of our perturbative approach, the magnitude of the scattering rate scales di-

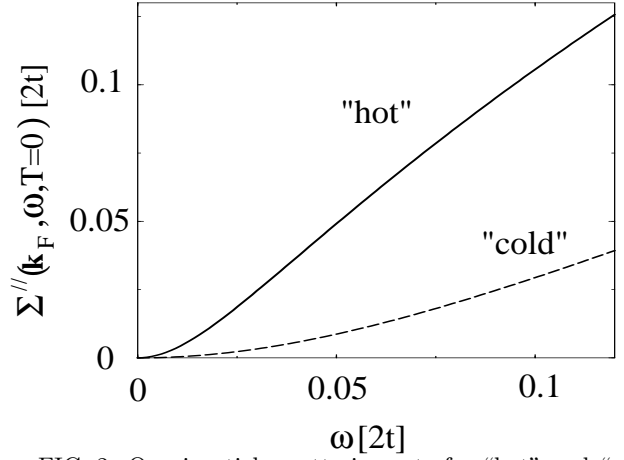


FIG. 2. Quasiparticle scattering rate for “hot” and “cold” spots on the Fermi surface as a function of frequency for  $T = 0$ . The “hot” spot corresponds to  $\mathbf{k}_{\mathbf{F}} = (3.026, 0.4817)$  while the “cold” spot corresponds to  $\mathbf{k}_{\mathbf{F}} = (1.107, 1.107)$ . Here the  $z = 1$  parameters as given in the caption of in Fig. 1 are used.

rectly with  $\alpha g^2$ . The band structure parameters are chosen to be most applicable to slightly overdoped systems:  $t'/t = 0.45$  and a filling  $\langle n \rangle = 0.8$ . The other parameters of the theory are chosen to provide a smooth link from the  $z = 2$  to the  $z = 1$  scaling regimes, as defined in the figure caption.

Fig. 1 shows that the scattering rate is extremely anisotropic around the Fermi surface, having “hot regions” (near the zone axes) where the qp scattering rate is peaked, and “cold regions” (near the zone diagonals) where the rate is smallest. The difference between the scattering at the “hot” and “cold” regions is smallest at high temperatures, and is due largely to the enhanced density of states near the zone axes. As the temperature cools the “hot spots” become more developed and more strongly peaked as a function of momentum. This is due to the interaction being more and more peaked for momentum transfers near  $(\pi, \pi)$  as the temperature cools. Thus the “hot spots” are those regions of the Fermi surface which can be connected by the AF wave-vectors  $\mathbf{Q} = (\pm\pi, \pm\pi)$ . These regions are close to the zone axes for the given band structure, and the  $B_{1g}$  geometry most effectively probes these hot spots while the  $B_{2g}$  geometry probes along the zone diagonals and therefore sees “colder” qps.

Next we consider the frequency dependence of the scattering rate away from the Fermi level. This is shown in Fig. 2, where the qp scattering rate at  $T = 0$  is plotted for both “hot” and “cold” qps, as defined in the figure caption. Both scattering rates vary as  $\omega^2$  at small  $\omega$ , characteristic of a Fermi liquid, but cross over to a behavior which is effectively linear in  $\omega$  at larger frequencies. For the “hot” qps this crossover happens at smaller values of  $\omega$  (0.025, in units of  $2t$ ) than for the “cold” qps (0.092). Moreover, the scattering is once again larger for the “hot” spots than for the “cold”. Similar results

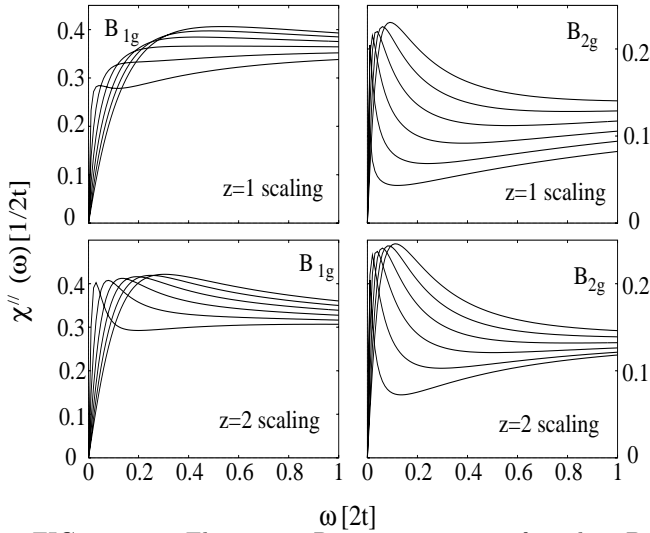


FIG. 3. Electronic Raman response for the  $B_{1g}$  and  $B_{2g}$  channels evaluated at different temperatures ( $T/2t = 0.01, 0.02, \dots, 0.06$  from top to bottom) for the  $z = 1$  and the  $z = 2$  scaling regimes of NAFL theory. Here we have set  $b_1 = b_2 = 1$ , as defined in the text.

have been obtained in Ref. [20,19], and the reader is directed to that reference for further details. From the point of view of Raman scattering, we would expect that the different magnitude and frequency/temperature dependence of the scattering rate around the Fermi surface will be manifest in the Raman response.

## 2. Channel dependent Raman response.

Considering the Raman response, we see that the  $B_{1g}$  part of the spectra probes the “hot regions” of large qp scattering while  $B_{2g}$  probes the “cold regions”. This means that the  $B_{1g}$  response should probe less coherent quasiparticles than the  $B_{2g}$  response, which should be reflected in the temperature dependence and general lineshape of the Raman continuum.

Within our perturbative approach we present in Fig. 3 the results for the  $B_{1g}$  and  $B_{2g}$  Raman response functions for both  $z = 1$  and  $z = 2$  scaling regimes. The parameters we have used for both scaling regimes are  $g = 1\text{eV}$ ,  $\alpha = 3.1$  states/eV,  $t = 250\text{meV}$ ,  $t'/t = 0.45$ , filling  $\langle n \rangle = 0.8$ ,  $\gamma_{B_{1g}}(\mathbf{k}) = b_1[\cos(k_x) - \cos(k_y)]$ ,  $\gamma_{B_{2g}}(\mathbf{k}) = b_2 \sin(k_x) \sin(k_y)$ . In addition, for the  $z = 1$  scaling regime we have used  $\omega_{sf}\xi = 50\text{meV}$  and  $\xi^{-1} = 0.1 + 4.64T/2t$ , while for the  $z = 2$  scaling regime,  $\omega_{sf}\xi^2 = 60\text{meV}$  and  $\omega_{sf}/2t = 0.0237 + 0.55T/2t$ . These parameters are similar to those used in Ref. [20] to describe the Hall conductivity data in  $\text{YBa}_2\text{Cu}_3\text{O}_7$ . Here the absolute magnitude for the scattering is arbitrary and determined by the dimensionless coefficients  $b_1$  and  $b_2$ , which are set by fitting to the data. This has no effect on the frequency dependent lineshapes, however.

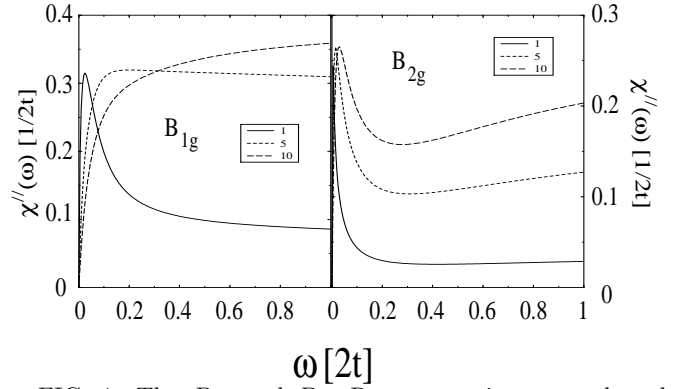


FIG. 4. The  $B_{1g}$  and  $B_{2g}$  Raman continua are plotted for  $T/2t = 0.03$  for values of the effective coupling constant  $g_{eff} = 1, 5, 10$ , as defined in the text. The  $z = 1$  parameters were used for  $\omega_{sf}$  and  $\xi$  as in Fig. 3.

The spectra for both scaling regimes share several features. First, the flat continuum at high frequencies which is present in the Raman data from all cuprate superconductors is reproduced by the theory. This is a consequence of a scattering rate  $\Sigma''(\omega)$  which is effectively linearly dependent on  $\omega$  at frequency scales larger than  $\omega_{sf}$ , as shown in Fig. 2. More importantly, the Raman response is different for the two scattering geometries as a consequence of the strong anisotropy of the scattering rate in the Brillouin zone as shown in Fig. 1. First of all, the position of the peak of the spectra in the  $B_{1g}$  channel is at a larger frequency in all figures compared to the  $B_{2g}$  channel. This is due to the larger magnitude of scattering probed. Moreover, the  $B_{1g}$  spectra is overall flatter than the  $B_{2g}$  spectra. This is due to the frequency dependence of the scattering. As shown in Fig. 2, the scattering rate probed in the  $B_{1g}$  channel becomes effectively linear in frequency at a much smaller frequency than that probed by the  $B_{2g}$  channel. Thus the  $B_{1g}$  spectra becomes flatter at smaller Raman shifts than the  $B_{2g}$  spectra. Moreover, the spectra rise linearly with  $\omega$  with a smaller slope for large scattering than for weaker scattering. This explains the differences between the curves in Fig. 3 reflecting the larger qp scattering in the  $B_{1g}$  channel.

The differences between the  $z = 1$  and  $z = 2$  results are largely quantitative but once again show the influence of the anisotropy of the qp scattering. The  $B_{1g}$  spectra show the greater difference between the two scaling regimes, as the overall spectra appears flatter for  $z = 1$  than for  $z = 2$ . This is due to the more pronounced hot spots in the  $z = 1$  regime. The  $B_{1g}$  channel thus is more sensitive than the  $B_{2g}$  channel to the growth of the correlation length as temperature is lowered.

The role of the effective coupling constant is to determine the overall shape of the continuum. In agreement with earlier models in Section III A, an increase of the coupling constant leads to (1) an increase in the overall magnitude of the cross section, (2) flatter spectra, and (3) the movement of the weak peak of the spectra out to larger energy scales. This is shown in Fig. 4 which

plots the  $B_{1g}$  and  $B_{2g}$  Raman response as a function of frequency shift at low temperatures  $T/2t = 0.03$  for different values of  $g_{eff} = \alpha g^2/2t$ .

As a consequence, the sensitivity of the Raman spectra to the details of the parameters can be a very useful tool to probe the anisotropic qp scattering rates in much the same way as it has been used to probe the anisotropy of the energy gap  $\Delta(\mathbf{k})$  in the superconducting state [3].

#### IV. FIT TO OVERDOPED BI-2212.

As we remarked, the approximations used ( $i-iv$  listed in Section III B) are most appropriate for systems with weak spin fluctuation scattering, and therefore we expect that our results would best represent the data from appreciably over-doped cuprate superconductors. Before we consider the effects of a more consistent treatment of the interactions in NAFL beyond perturbation theory, it is useful to explore how the perturbative theory compares to the data on overdoped cuprates in their normal state.

For a comparison to these data we thus consider the results from the  $z = 2$  scaling regime in closer detail. As discussed in Ref. [3], it is believed that the qps in the over-doped cuprates feel a stronger impurity interaction coming from the increased effective dimensionality which allows the qps to interact more strongly with defects residing out of the  $\text{CuO}_2$  planes. Therefore in addition we will consider an isotropic impurity interaction  $H_{imp} = \sum_{\mathbf{k}, \mathbf{k}'} \sum_{i, \sigma} U e^{i(\mathbf{k}-\mathbf{k}') \cdot \mathbf{R}_i} c_{\mathbf{k}, \sigma}^\dagger c_{\mathbf{k}', \sigma}$ , where  $\mathbf{R}_i$  denotes the position of the impurity labeled by  $i$  and  $U$  is the impurity potential. After averaging over the position of the impurities, this adds a momentum independent term to the imaginary part of the self energy  $\Gamma_{imp} = \pi n_i N_F |U|^2$ , where  $n_i$  is the impurity concentration and  $N_F$  is the density of states per spin at the Fermi level.

The fit of the theory to the temperature dependent spectra for each channel obtained in over-doped Bi 2212 ( $T_c = 55K$ ) by Hackl et al. in Ref. [21] is shown in Fig. 5 for the  $B_{1g}$  and  $B_{2g}$  channels. We note that  $\omega_{sf}$  and  $\xi$  have so far not been determined via fits to magnetic response data. These fits are thus obtained by choosing:  $\omega_{sf}$  and  $\xi$  at a fixed temperature, the magnitude of the impurity scattering rate, a magnitude of the coupling constant  $\alpha g^2$ , and lastly  $b_1$  and  $b_2$ . Then, only the temperature dependent part of  $\omega_{sf}$  was modified to fit the data at other temperatures. The parameters we have used are  $b_2/b_1 = 0.417$ ,  $\Gamma_{imp} = 40\text{cm}^{-1}$ ,  $\omega_{sf}\xi^2 = 13\text{meV}$ , and  $\omega_{sf} = 160K + 0.06T[K]$ .

Further information can be obtained from the slope of the spectra at vanishing frequencies. We denote this slope as  $\Gamma_\lambda = \lim_{\Omega \rightarrow 0} \Omega/\chi''_\lambda(\Omega)$ , for  $\lambda = B_{1g}$  or  $B_{2g}$ . In Ref. [21] it was shown that the inverse of this slope has qualitatively different behaviors for different doping regimes of various cuprate materials. While the inverse slope observed in the  $B_{2g}$  channel always was found to

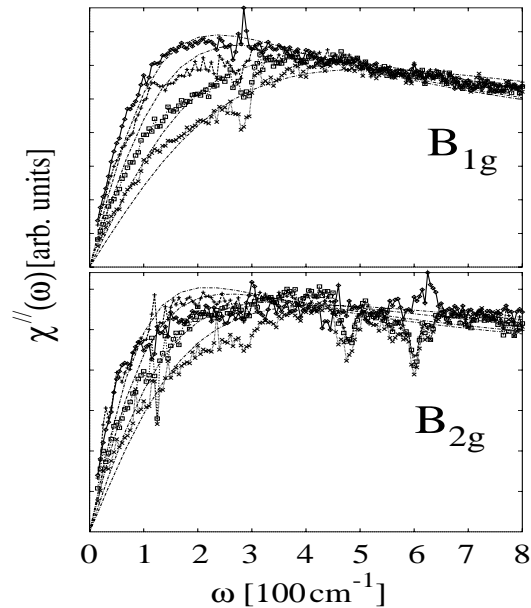


FIG. 5. Fit of the  $z = 2$  NAFL theory to the  $B_{1g}$  and  $B_{2g}$  spectra taken in [21] on over-doped  $\text{Bi}_2\text{Sr}_2\text{CaCu}_2\text{O}_{8+\delta}$  ( $T_c = 55K$ ) at  $60K, 90K, 150K,$  and  $200K$  from top to bottom. Parameters used are given in the text.

track the temperature dependence of the DC resistivity for all regions of doping, the  $B_{1g}$  inverse slope showed a remarkable sensitivity to doping. For overdoped systems, the  $B_{1g}$  slope was similar to the  $B_{2g}$  rate, and effectively followed the behavior  $\Gamma_{B_{1g}} \sim \Gamma_{B_{2g}} \sim \text{constant} + T^2$ . For optimally doped cuprates,  $\Gamma_{B_{2g}} \sim T$ , while  $\Gamma_{B_{1g}} \sim \text{constant}$ . Moreover, for underdoped materials the  $B_{1g}$  inverse slope was found to increase with decreasing temperature, indicative of insulating behavior.

Within the level of our approximations, the low frequency Raman response is given by

$$\frac{1}{\Gamma_\gamma(T)} = \lim_{\Omega \rightarrow 0} \chi''_{\gamma, \gamma}(\Omega)/\Omega = \int \frac{d\Omega_{\mathbf{k}}}{|\mathbf{v}_{\mathbf{k}}|} \gamma^2(\mathbf{k}) \int \frac{dx}{[2 \cosh(x/2)]^2} \frac{1}{\Sigma''(\mathbf{k}, xT)}. \quad (15)$$

Thereby, we see that the inverse slope effectively directly samples the qp scattering lifetime at regions of the Fermi surface selected by the light polarization orientations. It is important to note that in this level of approximations, the momentum dependence of the Raman vertices competes with the momentum dependent scattering rate on the Fermi surface, meaning that the largest contribution to the integral in Eq. (16) comes from where the Raman vertex is the largest and where the qp scattering rate is the smallest. Therefore, here the Raman inverse slope washes out direct information about the  $k$ -dependence of the scattering rate and leads to a more similar behavior of the  $B_{1g}$  and  $B_{2g}$  inverse slope, which hides the underlying anisotropy of the qp scattering rate. This is due to the approximations of restricting consideration to the Fermi surface only and to the neglect of vertex

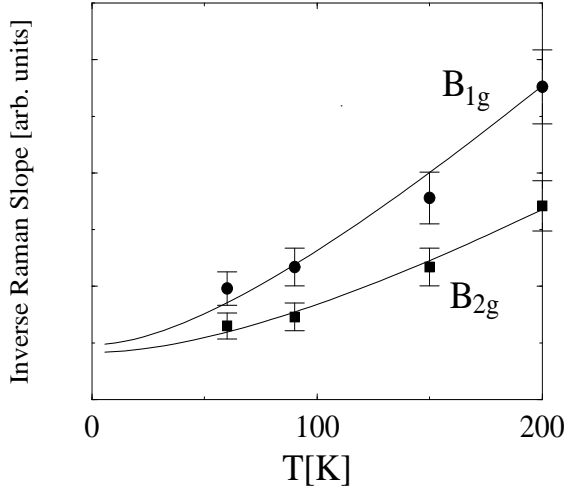


FIG. 6. Fit of the inverse slope of the Raman response for the two symmetry channels.

corrections. In the following section this is shown to be crucial if the spin fluctuations are strong.

However, for weak spin fluctuations, we believe that the data on overdoped materials can be best fit with this perturbative approach. In Fig. 6 we plot the inverse Raman slope obtained from the parameters used in Fig. 5 and compare the results to the data taken in [21]. The fit to the data is quite good when 8% error bars for the data [22] are taken into account. The data are consistent with a scattering rate which is not too anisotropic, and is governed by elastic scattering from impurities, and inelastic Fermi liquid like scattering. We remark that similar fits can be made with slightly different parameter choices than the ones considered here.

## V. SELF CONSISTENCY AND VERTEX CORRECTIONS.

While good agreement between the theory and the data has been shown for over-doped Bi 2212, several features remain to be explained in optimally and underdoped systems. As mentioned in the last section, the difference of the inverse slope of the Raman response between  $B_{1g}$  and  $B_{2g}$  channels grows remarkably upon lesser dopings [21]. Moreover, features which have been associated with a pseudo-gap have been observed in the under-doped systems [6]. Since our fits to the data were restricted by our approximations to weak spin fluctuations, we need an improved formalism for an insight into the effects of strong spin fluctuations.

Therefore for the remainder of the letter we solve the model lifting the restrictions ( $i - iv$ ) listed before. The calculations were performed by first solving for the Green's function Eq. (14) self consistently while maintaining a filling  $\langle n \rangle = 0.8$ . We used a hard frequency cutoff  $\omega^* = 0.4\text{eV}$  for the interaction Eq. (1) to improve

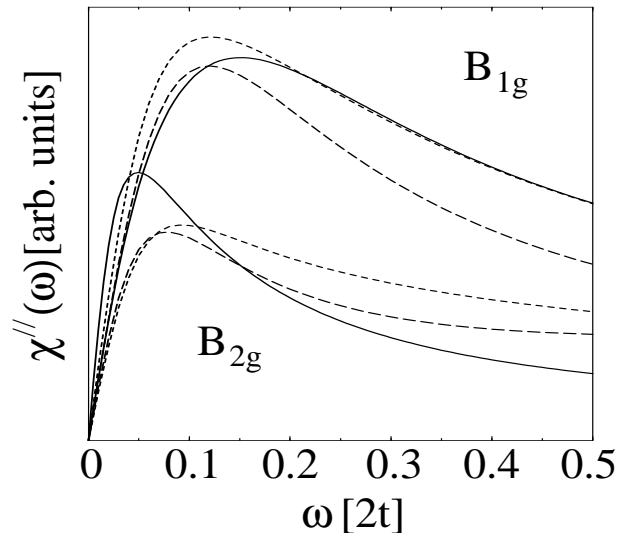


FIG. 7. Comparison of the results obtained from perturbation theory (solid line), self consistent treatment (short dashed line), and the additional inclusion of vertex corrections (long dashed lines).

convergence, but note that our results hardly were affected by this cutoff. Then the Bethe-Salpeter equation (10) was evaluated for the renormalized vertex. The calculations were carried out on the imaginary frequency axis using 256 Matsubara frequencies and  $64 \times 64$  to  $128 \times 128$   $\mathbf{k}$ -points. The integral equation for the vertex  $\tilde{\gamma}(\mathbf{k}, i\omega, i\omega + i\Omega)$  was solved for each external (internal) bosonic (fermionic) Matsubara frequency  $i\Omega$  ( $i\omega$ ). Once completed, the Raman response was evaluated using Eq. 10 and the results were analytically continued to the real frequency axis using Padé approximants [23]. Since the Raman response is in general quite featureless the Padé procedure was highly accurate (using 20-60 points changes the results by less than 5 %).

The results are summarized in Fig. 7 which compares the effects of self consistency and vertex renormalizations to the results from perturbation theory for  $T = 0.08t$ .  $\omega_{sf}$ ,  $\xi$ , and  $g_{eff}$  were chosen for the  $z = 2$  scaling regime as in Fig. 3. We first discuss the differences between a perturbative (solid lines in the figure) and self consistent treatment (short dashed lines). By noting that the position of the peak in the  $B_{1g}$  channel decreases in frequency while the  $B_{2g}$  peak position increases under self consistency, it can be seen that the effect of a self consistent treatment is to decrease the relative anisotropy in the scattering rate around the Fermi surface, leading to a more effectively “isotropic-like” response which places the peak of the spectra at nearly the same position ( $\sim 0.2t$ ) for both channels. The smoothing out of the scattering also leads to a  $B_{1g}$  spectrum which is slightly narrower in profile than the perturbation results, while the  $B_{2g}$  spectrum is wider. Although we have not tried to fit the self consistent theory to the data on overdoped Bi 2212 in Fig. 5, it appears that if disorder is once again added, an equally good fit would be obtained us-

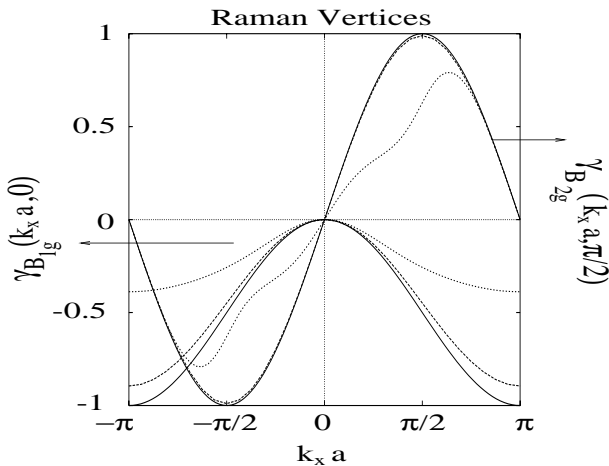


FIG. 8. Renormalization of the Raman vertices for the two symmetry channels evaluated for the lowest bosonic Matsubara frequency. The data sets correspond to the bare vertices, the renormalized vertices for the  $z = 2$  (over-doped) data set as in Fig. 3, and the renormalized vertices corresponding to the  $z = 1$  (under-doped) data set, in descending order, respectively. For the  $z = 1$  set, the value of  $\alpha = 16.7$  states/eV, corresponding to  $\text{YBa}_2\text{Cu}_3\text{O}_{6.5}$  [19].

ing a slightly larger value of the coupling constant  $g_{eff}$  to offset the reduction due to self consistency. We note however that the self consistent treatment would not yield a particularly good fit to the data on optimally and under-doped systems, which show much more anisotropy than that indicated in Fig. 7.

This can be partially offset by interaction renormalization of the Raman vertex. When the vertex corrections are included, the  $B_{1g}$  spectrum is most affected, with an overall reduction intensity occurring over a wide region of frequencies. This can be seen more clearly by examining the Raman vertices directly. In Fig. 8 we plot the  $B_{1g}$  and  $B_{2g}$  vertices for selected directions in the Brillouin Zone for different values of the coupling  $g_{eff}$  and different scaling regimes. The  $z = 2$  curves correspond to the parameters used in Figs. 3 and 7, while the  $z = 1$  curves correspond to the values used for  $\text{YBa}_2\text{Cu}_3\text{O}_{6.5}$  in [19], with  $\alpha = 16.7$  states/eV. Since  $g = 1$  eV and  $t = 250$  meV has been used for all curves,  $g_{eff} = \alpha g^2 / 2t = 6.2(33.4)$  for the  $z = 2(z = 1)$  curves in Fig. 8. We found no cases of symmetry mixing and the renormalized vertices retain their bare group transformation properties. Compared to the bare vertices, the  $B_{1g}$  vertex shows much more of reduction than the  $B_{2g}$  vertex. The renormalized vertex  $\tilde{\gamma}$  for the  $B_{1g}$  channel is reduced in particular near the zone axes or “hot spots”. However, the  $B_{2g}$  vertex is hardly affected by the vertex renormalizations. This is consistent with the effects of a “cold” interaction probed along the zone diagonals. As the interaction is increased, the  $B_{1g}$  vertex is reduced dramatically near the “hot spots”. The  $B_{1g}$  vertex is reduced by a factor 2 near the “hot spots” compared to its bare value, while the  $B_{2g}$  vertex is reduced by a

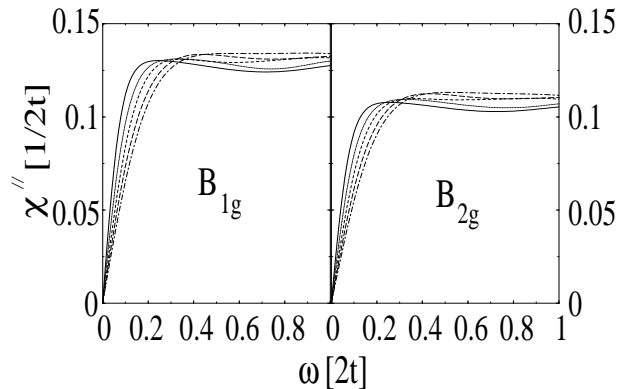


FIG. 9. The full Raman response (evaluated with self consistency and vertex renormalization) at temperatures  $T/2t = 0.03$  (solid),  $0.04$  (dotted),  $0.5$  (dashed),  $0.6$  (long-dashed),  $0.7$  (short-dashed), for the  $B_{1g}$  and  $B_{2g}$  channels. The parameters used corresponding to values for  $\text{YBa}_2\text{Cu}_3\text{O}_{6.5}$  [19].

smaller value,  $\sim 75\%$ , and has a peak which is shifted out towards the “hot spots”. Since the Raman vertex renormalization enters with the opposite sign as the self energy vertex correction, these results complement the results of Ref. [24] which showed that the effect of vertex corrections *on the interaction* yields an effectively weaker coupling constant.

The vertex renormalization should suppress the  $B_{1g}$  cross section compared to the  $B_{2g}$  cross section for larger interaction strengths. Since the  $B_{2g}$  vertex is affected less dramatically, the net effect would appear that the  $B_{2g}$  cross section remains relatively unchanged with increasing interaction, while the  $B_{1g}$  overall cross section comes down in magnitude to be closer to the  $B_{2g}$  value. We remark that this trend is consistent with the data from the cuprates which show a large decrease of the  $B_{1g}$  to  $B_{2g}$  ratio of the Raman spectra upon under-doping [6] which we relate to the growth of “hot spots” intensity and subsequently large vertex renormalizations.

This can be seen more clearly in Fig. 9, which shows the full Raman response for larger values of the coupling  $g_{eff}$  corresponding to  $\text{YBa}_2\text{Cu}_3\text{O}_{6.5}$  [19]. The spectra are much flatter than those calculated for smaller coupling constants, and appear to differ only quantitatively. The effect of the anisotropy of the scattering rate appears to have been washed out due to self consistency, as the spectra have a “shoulder” at the same frequency and show roughly the same temperature dependence. However, the overall magnitude of the spectra at larger frequency shifts is reduced for the  $B_{1g}$  spectra relative to the  $B_{2g}$  spectra, leading to a ratio of the continua nearly equal to 1. As indicated in Fig. 8, this is entirely due to the vertex renormalization. While the relative magnitude of the continua and overall lineshape is similar to that seen in experiments at a single temperature [6], the temperature dependence seen in experiments is qualitatively different.

This can be explored in more detail by plotting in Fig.

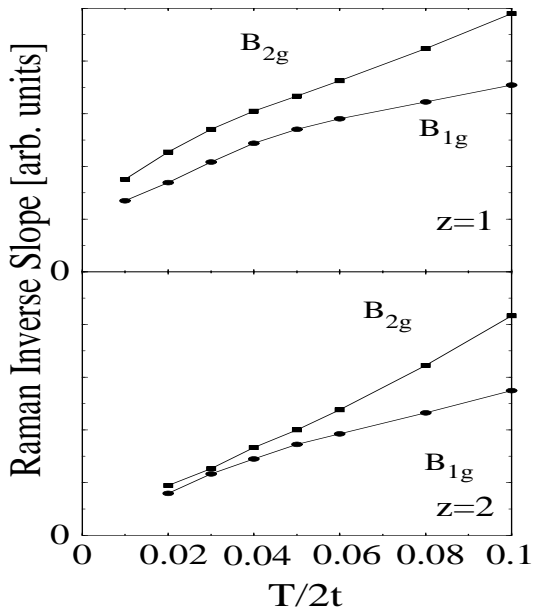


FIG. 10. The temperature dependence of the Raman inverse slope calculated self consistently with vertex corrections evaluated for both symmetries and scaling regimes.

the inverse slope of the Raman spectra for the self consistent and vertex corrected calculation. These results are qualitatively different from the perturbative treatment as discussed earlier. From Eq. (16) the inverse Raman slope has the same behavior as the qp scattering rate at zero frequency. If no disorder is included then the inverse Raman slope varies as  $T^2$  below a characteristic  $T^*$  and crosses over to  $T$  at larger temperatures.  $T^*$  is connected with  $\omega_{sf}$ , and is generally dependent on parameter choices. However Fig. 10 shows that the vertex corrected, self consistent treatment does not show similar behavior. For the  $z=2$  scaling regime, the inverse slope is proportional to  $T$  down to the lowest temperatures reachable for our level of numerical accuracy, while for the  $z=1$  regime, the inverse slope appears to extrapolate to a non-zero value at  $T=0$ . A simple connection between these and the perturbative results is that the self consistency leads to a strong downward renormalization of  $\omega_{sf}$  and a much lower crossover  $T^*$  to Fermi liquid-like behavior. The renormalization is stronger for the  $z=1$  case than  $z=2$ , in agreement with our earlier discussion. Our results thus indicate that the inverse slope should fall as  $T$  is decreased until  $\sim T_{cr}$  which separates the  $z=1$  and  $z=2$  scaling behavior. Then the slope should flatten out and become roughly constant. To check this it would be useful to explore the inverse Raman slope as a function of temperature for more systems at different dopings. Such a behavior has been reported by Naeini *et al.* in slightly overdoped  $\text{La}_{1-x}\text{Sr}_x\text{CuO}_4$  [25].

While this behavior is similar to what has been observed in the  $B_{2g}$  channel, the theory does not predict a considerable difference for the  $B_{1g}$  channel. Experimentally, the  $B_{1g}$  channel shows an inverse slope for op-

timally doped materials that is essentially temperature independent, and for underdoped materials, even grows with decreasing temperature. From our calculations, it appears that the effect of self consistency obscures the anisotropy inherent in the model, leading to a temperature dependent behavior which is similar for both channels. While the effect of vertex corrections appears to heighten the anisotropy, as shown in Fig. 8, the self consistency appears to dominate the response, as seen in Fig. 10. It would appear then that a treatment which neglected self consistency and focused only on vertex renormalizations would lead to a more apt description of the experiments. This remains to be explored.

## VI. SUMMARY AND CONCLUSIONS

In summary we have seen how anisotropic qp scattering leads to manifestly channel dependent Raman cross sections and how through a careful examination of the temperature dependence of the spectra, important information can be extracted concerning anisotropic qp dynamics. The coherence or incoherence of the qp's spectral function can be probed directly via Raman scattering, thereby offering an additional avenue besides ARPES to explore momentum resolved qp information. Signatures of a strong interaction are: (1) the position of a weak peak in the spectrum occurring at large frequency shifts, and (2) the increased overall magnitude of the spectra. If the interaction is strongly anisotropic, both features can be different for different polarization channels. The qp dynamics can be probed by examining the temperature dependence of both the low and high frequency portions of the channel dependent Raman response. For the cuprates, the consequence of an interaction which scatters qps with relative momentum of the antiferromagnetic lattice vector  $\mathbf{Q}$  are (1) a stronger overall signal, (2) a peak at higher frequencies, and (3) a weaker temperature dependence of the slope of the response in the  $B_{1g}$  channel compared to the  $B_{2g}$  channel.

Excellent agreement of the NAFL model was found with the Raman results on overdoped Bi 2212 (and La 214 [25]). With the inclusion of impurity scattering, the Raman response calculated in a perturbative way in NAFL yields a correct description of the spectra at a variety of temperatures. Improvements to the theory can be made with more accurate determination of the parameters of the theory via other experimental probes.

The effect of a more self consistent treatment leads to an overall reduction of anisotropy effects and a more isotropic Raman response, in contradiction to the experiments on optimally- and under-doped cuprates, at least for the  $B_{1g}$  channel. The self consistency yields a much weaker Fermi liquid-like behavior than that obtained via a perturbative approach. However, the theory does not adequately describe the larger relatively incoherent scattering probed by the  $B_{1g}$  light orientations. Improve-

ments can be made by once again exploring different parameter choices, but the nearly temperature independence of the  $B_{1g}$  response seen in the cuprates must be obtained by tuning both  $\omega_{sf}$  and  $\xi$  to have a strongly increasing interaction peaked near  $(\pi, \pi)$  transfers to offset the loss of phase space for qp scattering as the temperature is lowered. This remains to be explored.

Interestingly, the role of vertex corrections may help to obtain such a behavior. For larger couplings, the vertex corrections were found to be particularly large near the “hot spots” and led to a subsequently reduced vertex and overall signal for  $B_{1g}$  polarizations. Only a small change was seen for the  $B_{2g}$  channel. This general behavior has been observed in Y 123 and La 214, and has been attributed to the opening of a pseudo-gap. More than likely it would be important to also employ vertex corrections to the self energy and to go beyond the simple calculations as performed here. Diagrammatically we have evaluated the lowest order diagrams for the self energy, and we include the interactions in the Raman response through uncrossed vertex corrections (ladder approximation). We do not expect that these calculations can describe very strong spin fluctuations, but our approach in principle should give us an insight as to what is the most important physics we might expect as the strength of the spin fluctuations is increased by removing oxygen. This remains an open challenge.

#### ACKNOWLEDGMENTS

The authors would like to thank M. Opel, R. Nemetschek, and R. Hackl for making the data presented in Fig. 5 available to us prior to publication. T.P.D. would like to acknowledge helpful conversations with D. Pines, J. Schmalian, and B. Stojković. Acknowledgment (T.P.D.) is made to the Donors of the Petroleum Research Fund, administered by the American Chemical Society, for partial support of this research.

- 
- [1] D.S. Marshall, D. S. Dessau, A. G. Loeser, C.-H. Park, A. Y. Matsuura, J. N. Eckstein, I. Bozovic, P. Fournier, A. Kapitulnik, W. E. Spicer, and Z.-X. Shen, *Phys. Rev. Lett.* **76**, 4841 (1996).
- [2] A. G. Loeser, Z.-X. Shen, D. S. Dessau, D. S. Marshall, C. H. Park, P. Fournier, and A. Kapitulnik, *Science* **273**, 325 (1996); H. Ding, M. R. Norman, T. Yokoya, T. Takeuchi, M. Randeria, J. C. Campuzano, T. Takahashi, T. Mochiku, and K. Kadowaki, *Phys. Rev. Lett.* **78**, 2628 (1997).
- [3] T. P. Devereaux, D. Einzel, B. Stadlober, R. Hackl, D. H. Leach, and J. J. Neumeier, *Phys. Rev. Lett.* **72**, 396 (1994). For a recent review, see T. P. Devereaux and A. P. Kampf, *Int. J. Mod. Phys. B* **11**, 2093 (1997).
- [4] G. Blumberg, P. Abbamonte, M. V. Klein, W. C. Lee, D. M. Ginsberg, L. L. Miller, and A. Zibold, *Phys. Rev. B* **53**, R11930 (1996); D. Einzel and R. Hackl, *J. Raman Spectroscopy* **27**, 307 (1996); D. Reznik, S. L. Cooper, M. V. Klein, W. C. Lee, D. M. Ginsberg, A. A. Maksimov, A. V. Puchkov, I. I. Tartakovskii, and S.-W. Cheong, *Phys. Rev. B* **48**, 7624 (1993).
- [5] R. Hackl, M. Opel, P. F. Müller, G. Krug, B. Stadlober, R. Nemetschek, H. Berger, and L. Forró, *J. Low Temp. Phys.* **105**, 733 (1996).
- [6] X. K. Chen, J. G. Naeni, K. C. Hewitt, J. C. Irwin, R. Liang, and W. N. Hardy, *Phys. Rev. B* **56**, R513 (1997); R. Nemetschek, M. Opel, C. Hoffmann, P. F. Müller, R. Hackl, H. Berger, L. Forró, A. Erb, and E. Walker, *Phys. Rev. Lett.* **78**, 4837 (1997); G. Blumberg, M. Kang, M. V. Klein, K. Kadowaki, and C. Kendziora, *Science*, **278**, 1427 (1997).
- [7] L. B. Ioffe and A. J. Millis, preprint [cond-mat/9801092].
- [8] Z.-X. Shen and J. R. Schrieffer, *Phys. Rev. Lett.* **78**, 1771 (1997); J. Altmann, W. Brenig, and A. P. Kampf, preprint cond-mat 9707267.
- [9] A. Millis, H. Monien, and D. Pines, *Phys. Rev. B* **42**, 167 (1990).
- [10] M. V. Klein and S. B. Dierker, *Phys. Rev. B* **29**, 4976 (1984); H. Monien and A. Zawadowski, *Phys. Rev. B* **41**, 8798 (1990).
- [11] J. Kosztin and A. Zawadowski, *Solid State Commun.* **78**, 1029 (1991).
- [12] A. A. Abrikosov and V. M. Genkin, *Zh. Eksp. Teor. Fiz.* **40**, 842 (1973) [*Sov. Phys. JETP* **38**, 417 (1974)].
- [13] There are some exceptions - G. Blumberg, Moonsoo Kang, and M. V. Klein, *Phys. Rev. Lett.* **78**, 2461 (1997).
- [14] P. Allen, *Phys. Rev. B* **13**, 1416 (1976).
- [15] In the effective mass approximation Eq. (11) yields  $a_0 = 0$ ,  $a_2 = 2t$ ,  $a_4 = -8t'$  and  $a_6 = 8t''$ .
- [16] A. Zawadowski and A. Cardona, *Phys. Rev. B* **42**, 10732 (1990).
- [17] A. Virosztek and J. Ruvalds, *Phys. Rev. B* **45**, 347 (1992).
- [18] A. V. Chubukov, D. Pines, and B. P. Stojković, *J. Phys. Condens. Matter* **8**, 10017 (1996).
- [19] D. Pines *et al.*, to appear in *Rev. Mod. Phys.*
- [20] D. Pines and B. Stojković, *Phys. Rev. B* **55**, 8576 (1997); **56**, 11931 (1997).
- [21] R. Hackl, G. Krug, R. Nemetschek, M. Opel, and B. Stadlober, in *Spectroscopic Studies of Superconductors*, I. Bozovic and D. van der Marel, Eds., Proc. SPIE 2696, 194 (1996).
- [22] M. Opel, private communication.
- [23] J. Vidberg and J. Serene, *J. of Low Temp. Phys.* **29**, 179 (1977).
- [24] A. V. Chubukov, P. Monthoux, and D. Moor, *Phys. Rev. B* **56**, 7789 (1997); J. Schmalian, private communication.
- [25] J. G. Naeni, X. K. Chen, K. C. Hewitt, J. C. Irwin, T. P. Devereaux, M. Okuya, T. Kimura, and K. Kishio, *Phys. Rev. B* **57**, R11077 (1998).